Check for updates

AGU ADVANCING EARTH AND SPACE SCIENCE

Geophysical Research Letters®

RESEARCH LETTER
10.1029/2022GL100058

**Key Points:**

- Larger catchments within the Greenland Ice Sheet's ablation area impart significant delays on the timing of meltwater delivery to moulins
- Longer delays in meltwater delivery to moulins caused peak moulin head to occur 1–3.25 hr later in the day at higher elevations
- Peak moulin head and peak sliding speeds are not coincident at higher elevations where moulin density is low

**Supporting Information:**

Supporting Information may be found in the online version of this article.

**Correspondence to:**

J. Z. Mejia,
jzmejia@buffalo.edu

**Citation:**

Mejia, J. Z., Gulley, J. D., Trunz, C., Covington, M. D., Bartholomaus, T. C., Breithaupt, C., et al. (2022). Moulin density controls the timing of peak pressurization within the Greenland Ice Sheet's subglacial drainage system. *Geophysical Research Letters*, *49*, e2022GL100058. https://doi.org/10.1029/2022GL100058

Received 8 JUL 2022
Accepted 9 NOV 2022

**Author Contributions:**

**Conceptualization:** J. Z. Mejia, J. D. Gulley, C. Trunz, M. D. Covington
**Data curation:** J. Z. Mejia, C. Trunz, M. D. Covington
**Formal analysis:** J. Z. Mejia, C. Trunz, M. D. Covington, T. C. Bartholomaus, S. Xie
**Funding acquisition:** J. D. Gulley, M. D. Covington, T. H. Dixon
**Methodology:** J. Z. Mejia, J. D. Gulley, C. Trunz, M. D. Covington, T. C. Bartholomaus, C. Breithaupt, S. Xie
**Project Administration:** J. D. Gulley
**Resources:** J. D. Gulley, C. Trunz, M. D. Covington, T. C. Bartholomaus, T. H. Dixon
**Software:** J. Z. Mejia, M. D. Covington, T. C. Bartholomaus, S. Xie
**Supervision:** J. D. Gulley

© 2022. American Geophysical Union. All Rights Reserved.

# Moulin Density Controls the Timing of Peak Pressurization Within the Greenland Ice Sheet's Subglacial Drainage System

**J. Z. Mejia[1], J. D. Gulley[2], C. Trunz[3], M. D. Covington[4], T. C. Bartholomaus[5], C. Breithaupt[6], S. Xie[7], and T. H. Dixon[2]**

[1]Department of Geology, University at Buffalo, Buffalo, NY, USA, [2]Department of Geosciences, University of South Florida, Tampa, FL, USA, [3]College of Earth, Ocean, and Atmospheric Sciences, Oregon State University, Corvallis, OR, USA, [4]Department of Geosciences, University of Arkansas, Fayetteville, AR, USA, [5]Department of Earth and Spatial Sciences, University of Idaho, Moscow, ID, USA, [6]Exxonmobil Upstream Research Company, Spring, TX, USA, [7]Department of Civil and Environmental Engineering, University of Houston, Houston, TX, USA

**Abstract** Links between hydrology and sliding of the Greenland Ice Sheet (GrIS) are poorly understood. Here, we monitored meltwater's propagation through the glacial hydrologic system for catchments at different elevations by quantifying the lag cascade as daily meltwater pulses traveled through the supraglacial, englacial, and subglacial drainage systems. We found that meltwater's residence time within supraglacial catchments—depending upon area, snow cover, and degree of channelization—controls the timing of peak moulin head, resulting in the 2 hr later peak observed at higher elevations. Unlike at lower elevations where peak moulin head and peak sliding coincided, at higher elevations peak sliding lagged peak moulin head by ∼2.8 hr. This delay was likely caused by the area's lower moulin density, which required diurnal pressure oscillations to migrate further into the distributed drainage system to elicit the observed velocity response. These observations highlight the supraglacial drainage system's control on coupling GrIS subglacial hydrology and sliding.

**Plain Language Summary** Each summer, melting snow and ice collects within streams and rivers on the Greenland Ice Sheet's surface until reaching the bed through crevasses or moulins—near-vertical conduits that penetrate the entire ice thickness—where this meltwater can lubricate the bed, causing the overlying ice to slide more rapidly. Despite the important role of meltwater in modulating sliding speeds, little is known about how relationships between melting and sliding vary spatially or through time. Here, we take the novel approach of monitoring meltwater's propagation through the entire glacial hydraulic system at two elevations. We find that longer delays in the timing of meltwater delivery to moulins draining larger, higher-elevation catchments, caused peak moulin water level (i.e., peak pressurization) to occur 2 hr later in the day than at smaller, lower-elevation catchments. Unlike at lower elevations where peak moulin water level and sliding coincided, at higher elevations sliding lagged peak moulin water level by 2.8 hr. This delay was likely caused by the fewer number of moulins which require a single moulin to pressurize a larger area. This work reveals the importance of the supraglacial drainage system in controlling the timing of meltwater reaching the bed and its relationship with sliding.

## 1. Introduction

Accurate predictions of the Greenland Ice Sheet's (GrIS) future contributions to sea level rise require a good understanding of the dynamic links between melting, subglacial water pressures, and ice motion. Meltwater produced on the ice sheet's surface flows through complex networks of supraglacial streams and rivers that ultimately empty into crevasses or moulins (Rennermalm et al., 2013; Smith et al., 2015; Yang & Smith, 2016). Moulins are near-vertical conduits that can penetrate the entire ice thickness and connect to the most efficient parts of the dynamic subglacial drainage system (Gulley et al., 2012). Meltwater inputs to moulins modulate subglacial water pressures and basal traction, which controls sliding (e.g., Andrews et al., 2014, 2018; Badino & Piccini, 2002; Bartholomaus et al., 2007; Iken, 1972). In this way, the supraglacial, englacial, and subglacial drainage systems are inherently linked, meaning that changes in any of these components can impact ice motion. Despite the hydraulic system's interconnections, most studies of glacial hydrological systems have focused on one component at a time, resulting in critical gaps in our understanding of links between changes in hydrology and ice motion.

**Visualization:** J. Z. Mejia
**Writing – original draft:** J. Z. Mejia
**Writing – review & editing:** J. Z. Mejia, J. D. Gulley, C. Trunz, M. D. Covington, T. C. Bartholomaus, C. Breithaupt, T. H. Dixon

The supraglacial drainage system determines the timing and spatial distribution of meltwater inputs to the englacial and subglacial drainage systems. Frequently, the supraglacial drainage system is overlooked under the assumption that meltwater delivery to the subglacial drainage system is coincident with peak melting across the ablation area. Such simplifications contrast with observations that reveal significant heterogeneity in the timing of meltwater delivery to moulins (King, 2018; Yang & Smith, 2016; Yang et al., 2018), which can lag peak melting by up to 16 hr for the largest catchments (Smith et al., 2017). Observations show temporal lags between peak melting and peak sliding speeds increase with elevation and distance from the ice sheet's margin (Hoffman et al., 2011), suggesting there should be spatiotemporal differences in hydro-dynamic coupling throughout the GrIS ablation area. These lags are likely caused by longer delays in the timing of meltwater delivery to moulins with larger catchment areas, which similarly increase with elevation as moulin density decreases (Clason et al., 2015; Yang et al., 2018). Modeling work incorporating the spatial distribution of moulins (e.g., Banwell et al., 2016; de Fleurian et al., 2016; Ryser et al., 2014) has shown that spatial heterogeneity in moulin inputs influences the timing and seasonal evolution of the subglacial drainage system. Even though the importance of meltwater inputs on sliding is well documented, how the spatial distribution of moulins and differences in the timing of meltwater delivery to moulins impact sliding has not been fully investigated.

Here we take a novel and holistic approach to understanding relationships between melting and sliding on the GrIS by quantifying lags in meltwater propagation through each component of the glacial hydraulic system. We established two field camps at different elevations—a lower-elevation camp, *Low Camp*, and a higher-elevation camp, *High Camp*—where we measured the timing of daily peaks in melting, meltwater delivery to moulins, moulin hydraulic head (the water level within the moulin with respect to sea level), and surface ice velocity. We use these observations to investigate how differences in the physical characteristics of supraglacial drainage basins at different elevations control lags between peak meltwater production and peak delivery to moulins and how these differences impact sliding.

## 2. Data and Methods

In July 2017, we established two camps within the ablation area of Sermeq Avannarleq in west Greenland: a lower elevation site *Low Camp* and a higher-elevation site *High Camp* at elevations of 779 and 947 m.a.s.l., respectively (Figure 1; Table S2 in Supporting Information S1; Ice thicknesses of 503 and 790 m (Morlighem et al., 2017)). We monitored meltwater propagation within an internally drained catchment at each elevation, the moulins of which we refer to as JEME at Low Camp and RADI at High Camp (Figures 1b and 1c). We use this terminology to maintain consistency with existing literature (Covington et al., 2020; Mejia et al., 2021) and data archives (Mejia, Gulley, & Dixon, 2020; Mejia, Trunz, Covington, & Gulley, 2020; Mejia, Trunz, Covington, Gulley, & Breithaupt, 2020; Trunz et al., 2021). To constrain the timing and magnitude of daily melting we installed an automatic weather station at each camp (Text S3 in Supporting Information S1), supplementing our observations with data from the nearby GC-NET station JAR1 (Figure 1; Steffen et al., 1996). We monitored the timing of meltwater delivery to each catchment's terminal moulin using ultrasonic water level sensors positioned approximately 30 m upstream of each moulin (Text S4 in Supporting Information S1; Figures S1–S4 in Supporting Information S1). We measured moulin water level by directly instrumenting moulins with pressure transducers, allowing us to monitor pressure fluctuations within the most hydraulically connected parts of the subglacial drainage system (Text S5 in Supporting Information S1). On 21 July we instrumented Low Camp's JEME moulin (69.474°N, −49.825°E) which drained ∼0.2 km$^2$ (Figure 1; Table S1 in Supporting Information S1). On 29 July we instrumented High Camp's Radical moulin (RADI; 69.543°N, −49.693°E) which drained ∼16.7 km$^2$ (Figure 1; Tables S1 and S3 in Supporting Information S1). Finally, we monitored ice motion by installing global navigation satellite system (GNSS) station LMID at Low Camp and stations HMID and EORM at High Camp (Figures 1b and 1c; Text S6 in Supporting Information S1).

In 2018 we returned to the field to expand our observations. Before the onset of melting, we installed a seismic station to measure glaciohydraulic tremor amplitude, a proxy for the discharge and pressure gradient within subglacial conduits (Text S7 in Supporting Information S1; Bartholomaus et al., 2015; Gimbert et al., 2016), within Low Camp's main catchment JEME. On 10 July, we instrumented the newly formed PIRA moulin which drained the same catchment as JEME moulin the previous year (catchment area ∼0.2 km$^2$; Figure S3 in Supporting Information S1). PIRA moulin formed in approximately the same location as JEME moulin was before it had advected ∼90 m downglacier over the winter. To further constrain catchment area induced delays in meltwater



19448007, 2022, 22, Downloaded from https://agupubs.onlinelibrary.wiley.com/doi/10.1029/2022GL100058, Wiley Online Library on [07/06/2023]. See the Terms and Conditions (https://onlinelibrary.wiley.com/terms-and-conditions) on Wiley Online Library for rules of use; OA articles are governed by the applicable Creative Commons License

19448007, 2022, 22, Downloaded from https://agupubs.onlinelibrary.wiley.com/doi/10.1029/2022GL100058, Wiley Online Library on [07/06/2023]. See the Terms and Conditions (https://onlinelibrary.wiley.com/terms-and-conditions) on Wiley Online Library for rules of use; OA articles are governed by the applicable Creative Commons License

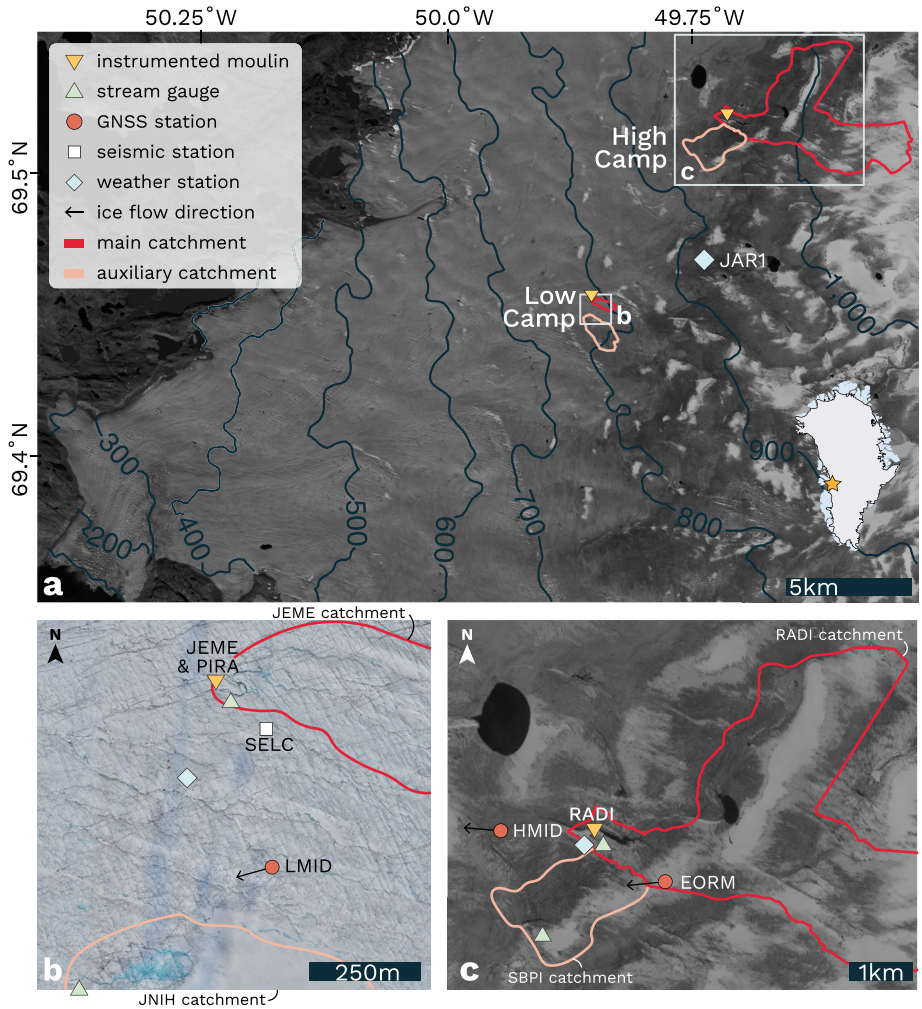



**Figure 1.** Sermeq Avannarleq field sites. (a) Sentine l-2 imagery from 10 Aug 2018 showing the full extent of the catchments studied at Low Camp and High Camp. (b) July 2018 drone orthophoto showing Low Camp, our main catchment JEME is outlined in red. PIRA (yellow triangle) and JEME moulins draining this catchment were located in the same position in 2017 and 2018 (Figures S1, S3, and S4 in Supporting Information S1). (c) High Camp zoom in showing instrumented moulin RADI (yellow triangle) with outlined catchments (Figures S2 and S5 in Supporting Information S1).

delivery to moulins, we instrumented two auxiliary catchments with supraglacial stream gauges: JNIH catchment at Low Camp (July 2017; area ~1.1 km$^2$), and SBPI catchment at High Camp (August 2018; ~2.4 km$^2$; peach outlines in Figure 1).

## 3. Results

The instruments deployed during the 2017 and 2018 melt seasons allowed us to monitor and constrain the timing of meltwater propagation through the glacial hydraulic system for catchments at Low Camp and High Camp. We deployed the first instruments in July 2017 after the melt season had already begun and the snowline had retreated past both our lower- and higher-elevation sites.

### 3.1. Meltwater Production

We used recorded meteorological measurements and the enhanced temperature-index model by Pellicciotti et al. (2005) to calculate melt rates to constrain the timing of peak meltwater production (Text S3 in Supporting Information S1; Figure 3a, Figures S9a–S11a in Supporting Information S1). Melting peaked simultaneously across our study area (Figure 2), occurring around 13:30 ± 1.4 hr local time (henceforth all times are reported in

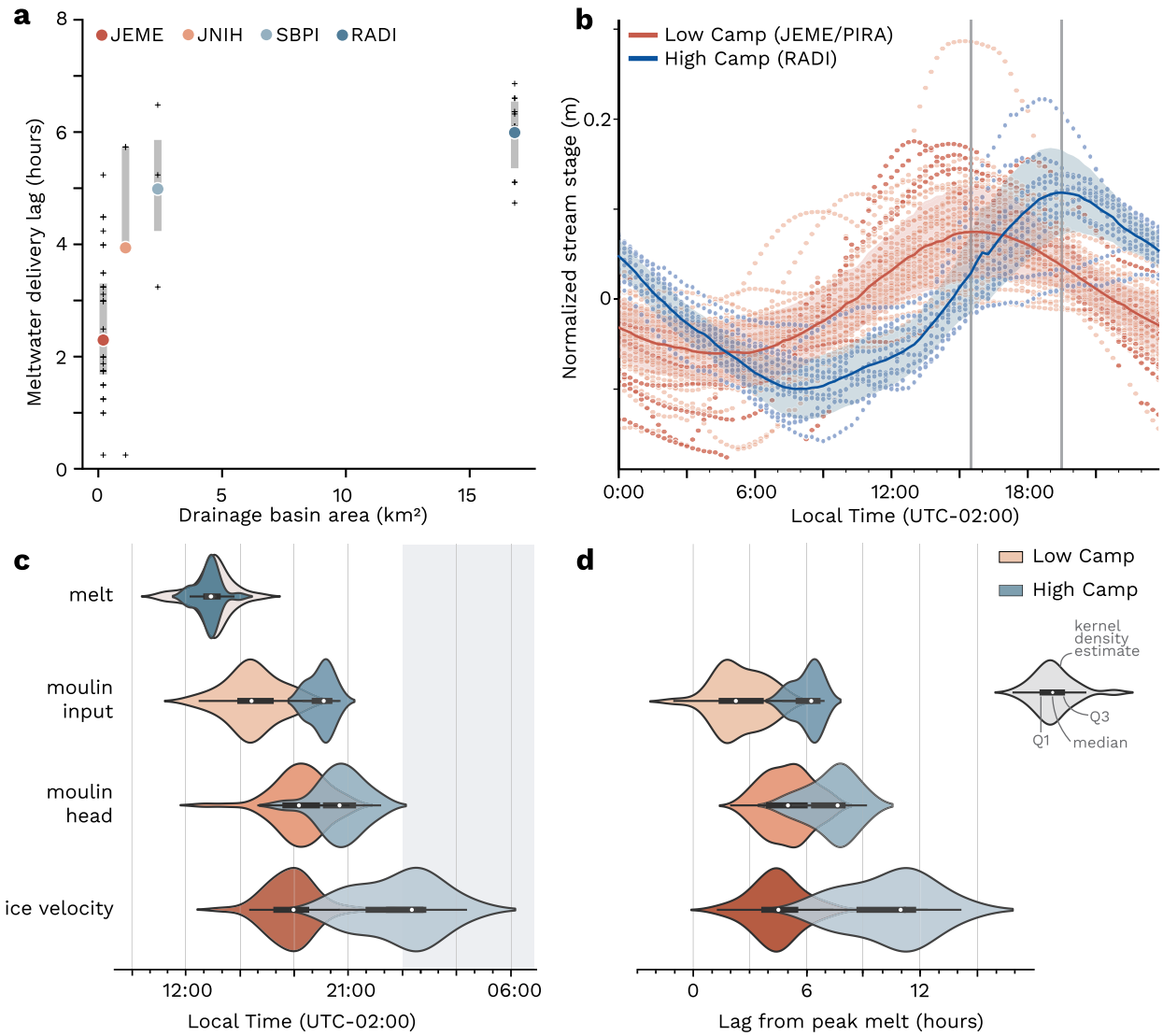



**Figure 2.** (a) Lag between peak melting and meltwater delivery to moulins plotted against catchment area. Circles mark the mean lag time in hours, gray bars denote $\pm 1\sigma$ standard deviation from the median (i.e., first and third quartiles), and individual observations are marked in black ($r = 0.67$, $p < 0.05$). (b) Normalized daily supraglacial stream stage for our primary catchments at Low Camp (orange) and High Camp (blue), solid lines mark mean values. The mean timing of diurnal peaks are marked with vertical gray lines for Low Camp (left) and High Camp (right). (c) Box plots overlaid by height-normalized kernel density estimates showing the timing of modeled peak melting, peak meltwater delivery to moulins, peak moulin head, and peak ice velocity for Low Camp (orange) and High Camp (blue) primary catchments during the 2017 melt season. Gray shading marks times after midnight (local time). (d) Same as in c but shown as lag from peak melting in hours.

local time, UTC-02:00). The timing and magnitude of peak melting was most strongly correlated with incoming solar radiation (Text S3 in Supporting Information S1), as was expected based on our choice of melt model. A comparison between calculated melt rate and ice surface ablation recorded at Low Camp (Text S3 in Supporting Information S1; 13 July–19 August 2017) shows good agreement with peak ablation occurring 13:30 ± 3.5 hr (Figures S7, S8 in Supporting Information S1). Over the same time period air temperature peaked 2 hr later, around 15:30 ± 3.3 hr (Figure S7 in Supporting Information S1). Moreover, peak melting occurred consistently around 13:30 at both Low Camp and High Camp over the 2017 and 2018 melt seasons. Due to the similarity in observations between weather stations, we use a single timeseries of peak melting to quantify lags across all variables (Figure 3a).



19448007, 2022, 22, Downloaded from https://agupubs.onlinelibrary.wiley.com/doi/10.1029/2022GL100058, Wiley Online Library on [07/06/2023]. See the Terms and Conditions (https://onlinelibrary.wiley.com/terms-and-conditions) on Wiley Online Library for rules of use; OA articles are governed by the applicable Creative Commons License

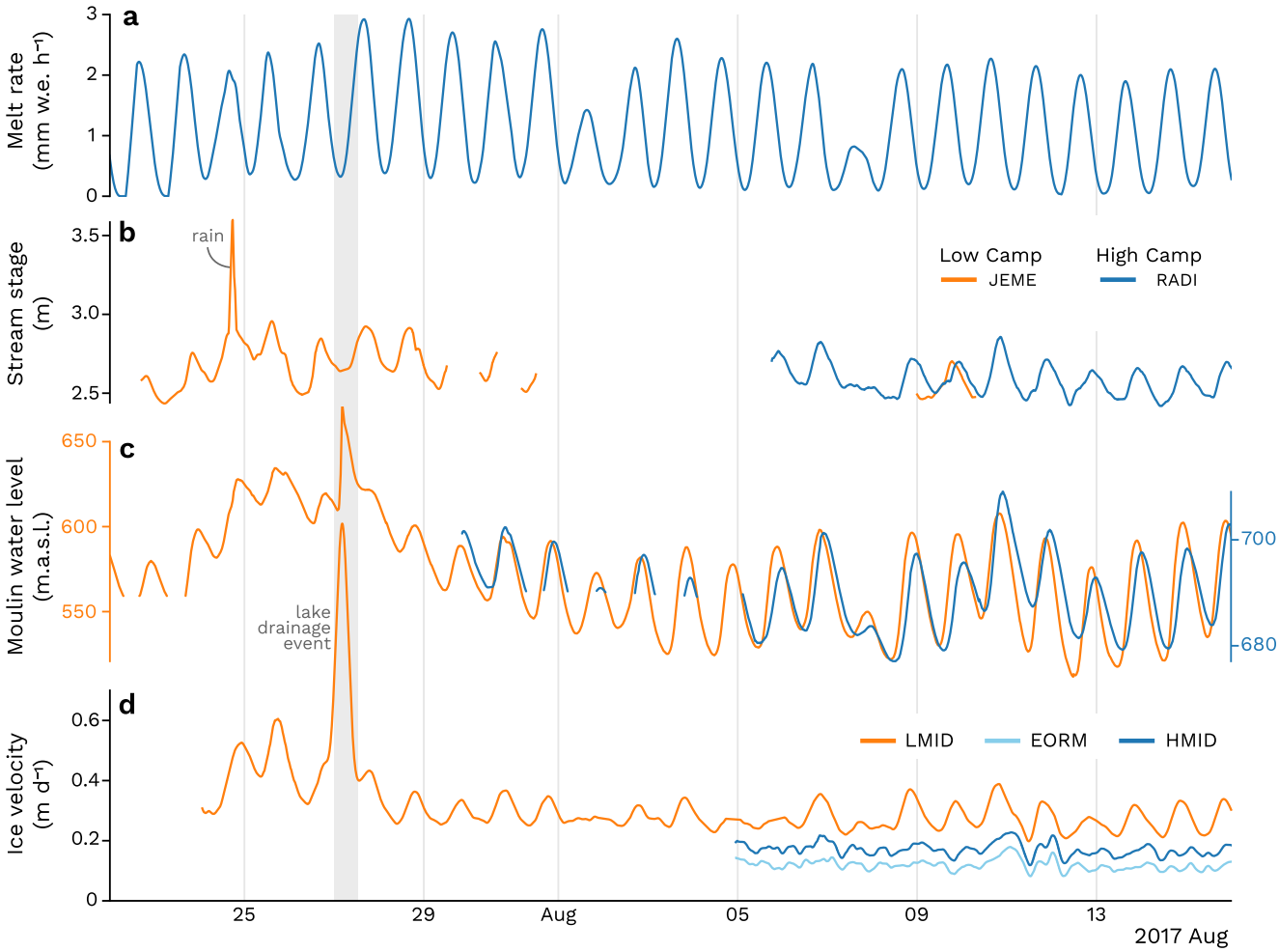



**Figure 3.** Comparison between Low Camp (orange) and High Camp (blue) meltwater propagation timeseries. (a) Modeled meltwater production across study area. (b) Supraglacial stream stage above an arbitrary datum. (c) Moulin hydraulic head from JEME moulin (left axis, orange) and RADI moulin (right axis, blue). Note that different scales are used to highlight the phase-shift between the two timeseries and better enable a visible comparison of the timing of diurnal moulin water level peaks (see Figure S12 in Supporting Information S1 for a single axis). (d) Along-flow ice velocity. Spikes associated with rainfall and lake drainage event are marked and are excluded from our analysis.

### 3.2. Meltwater Delivery to Moulins

Of the physical characteristics considered (catchment area, length, elongation ratio, and average surface slope), catchment area exerted the strongest controls on the timing of peak meltwater delivery to moulins (Figure 2a and Figure S17 in Supporting Information S1; Table S1 in Supporting Information S1; Text S2 in Supporting Information S1). Catchment length also had a strong correlation with the timing of peak meltwater delivery, mainly because of the strong correlation between catchment area and length ($r = 0.996$, $p < 0.005$) for the four catchments considered. At Low Camp's main catchment JEME (0.2 km$^2$), meltwater delivery peaked around 15:30 (Figures 2b and 2c), lagging peak melt by 2.4 ± 1.6 hr over the period of 2 July–9 August 2017 (Figure 2d; Table S3 in Supporting Information S1). At High Camp's much larger main catchment RADI (16.8 km$^2$), meltwater delivery peaked around 19:45, lagging peak melt by 6.5 ± 1.8 hr (Figure 2 and Figure S11 in Supporting Information S1) over the period of 5–16 August 2017. The longer residence time of meltwater within the supraglacial drainage system at the larger, higher-elevation catchment ultimately caused moulin input to peak four hours later in the day at High Camp than at Low Camp (Figures 2b and 2c). Importantly, all of the underlying data used to generate the aforementioned timing of peak meltwater delivery for our primary catchments were collected during bare-ice conditions (see Figures S1 and S2 in Supporting Information S1 for photos of surface conditions), after the seasonal snowpack had retreated upglacier past our sites. Bare-ice conditions therefore eliminate the influence of the seasonal snowpack on the timing of peak meltwater delivery to moulins reported here.



19448007, 2022, 22, Downloaded from https://agupubs.onlinelibrary.wiley.com/doi/10.1029/2022GL100058, Wiley Online Library on [07/06/2023]. See the Terms and Conditions (https://onlinelibrary.wiley.com/terms-and-conditions) on Wiley Online Library for rules of use; OA articles are governed by the applicable Creative Commons License

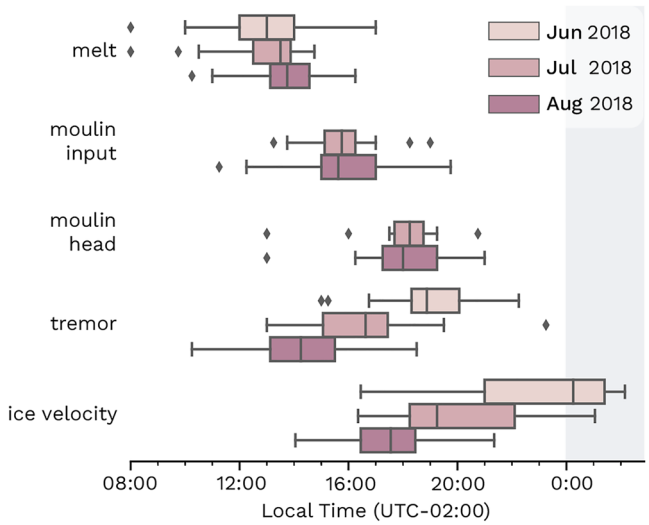



**Figure 4.** Seasonal shifts in meltwater propagation timing. Box and whisker plots show the monthly distribution of daily peaks in melting, meltwater input to PIRA moulin (stream stage), PIRA moulin head, tremor amplitude, and ice speed of Low Camp's JEME catchment during the 2018 melt season. Colors correspond to the month of the underlying data for June (lightest), July (mid-tone), and August (darkest). Gray diamonds mark outliers, and the center line corresponds to median values. Shading as in Figure 2.

Observations from our two auxiliary catchments confirm the pattern of longer lags between peak melting and peak meltwater delivery to moulins for larger catchments (Figure 2a; Table S1 in Supporting Information S1). At Low Camp's auxiliary catchment JNIH (1.1 km$^2$; 13–20 July 2017) peak meltwater delivery lagged peak melting by 4.2 ± 1.8 hr, and at High Camp's SBPI (2.4 km$^2$; August 2018) by 5.0 ± 1.3 hr. Lags between meltwater delivery to moulins and other catchment properties are presented in Figure S17 in Supporting Information S1. Altogether, observations from these four catchments indicate there are increasing delays in the timing of meltwater delivery to larger, higher-elevation catchments (Figure 2a) within this sector of the western GrIS.

### 3.3. Moulin Hydraulic Head and Sliding

Coincident timeseries of moulin head from August 2017 (Figure 3, Figures S9c–S11c in Supporting Information S1) constrain the timing of peak pressurization within the subglacial drainage system for Low Camp and High Camp moulins. The lag between peak meltwater delivery to moulins and peak moulin head was similar, approximately 2 hr, at both sites (Figures 2c and 2d). However, the longer delay in meltwater delivery caused High Camp's RADI moulin's water level to peak 1–3.25 hr later in the day than at the lower-elevation JEME moulin. This delay resulted in a clear phase shift between the moulin head timeseries from JEME and RADI moulins (Figure 3c).

We find a strong agreement between the timing of peak moulin head and peak sliding speed at Low Camp ($r = 0.86$, $p < 0.01$) that is not observed at High Camp ($r = 0.46$, $p < 0.01$; Figure S15 in Supporting Information S1). For example, peak sliding speed at Low Camp coincided with peak moulin head but lagged peak melting by 4.6 ± 1.7 hr (Figure 2d). This pattern was observed during 2017 and 2018 with peak sliding lagging peak moulin head by −0.4 ± 1.5 hr ($n = 21$) for JEME and −0.3 ± 2.3 hr ($n = 28$) for PIRA. While these negative lag times indicate peak sliding precedes peak moulin head, the associated uncertainties make these differences insignificant and these observations can be interpreted as moulin head and peak sliding peaking at approximately the same time at our Low Camp. In contrast, at High Camp peak sliding lagged (i.e., followed) peak moulin head by 2.8 ± 2.0 and 3.0 ± 1.2 hr for GNSS stations EORM and HMID respectively. Ultimately sliding peaked 2.2–7.6 hr later at High Camp than at Low Camp throughout the 2017 melt season (Figure 3d).

### 3.4. Glacio-Hydraulic Tremor Amplitude

To investigate how transient surface conditions (i.e., seasonal snowpack removal and supraglacial drainage network evolution) within Low Camp's JEME catchment influence the timing of meltwater delivery to moulins, we utilize observations of glacio-hydraulic tremor amplitude from seismic station SELC (Figure 1b). Specifically, we use tremor amplitude to monitor the timing of peak water flow within the subglacial drainage system, the timing of which should reflect surficial routing delays. The availability of seismic data during the beginning of the 2018 melt season supplements our stream stage data set covering the period from 11 July through 20 August 2018 during bare-ice conditions (Figure 4 and Figure S10 in Supporting Information S1). Our tremor amplitude timeseries spanned the entire duration of the melt season, from 5 June through the end of August 2018 ($n = 62$ for diurnal extrema picks). Peak meltwater delivery to PIRA moulin coincided with peak tremor amplitude (Figure S14 in Supporting Information S1; Text S4 and S7 in Supporting Information S1), which occurs when subglacial pressure gradients within moulin-connected subglacial channels are increasing most rapidly (Gimbert et al., 2016). From the monthly breakdown of diurnal extrema peaks shown in Figure 4, tremor amplitude peaked earlier in the day as the melt season progressed, lagging peak melting by 6.1 ± 2.2, 3.5 ± 2.5, and 1.4 ± 2.5 hr in June, July, and August respectively. These observations agree with stream stage measurements which show that the lag between peak melting and peak meltwater delivery decreased by 54 min between July and August 2018.



19448007, 2022, 22, Downloaded from https://agupubs.onlinelibrary.wiley.com/doi/10.1029/2022GL100058, Wiley Online Library on [07/06/2023]. See the Terms and Conditions (https://onlinelibrary.wiley.com/terms-and-conditions) on Wiley Online Library for rules of use; OA articles are governed by the applicable Creative Commons License

19448007, 2022, 22, Downloaded from https://agupubs.onlinelibrary.wiley.com/doi/10.1029/2022GL100058, Wiley Online Library on [07/06/2023]. See the Terms and Conditions (https://onlinelibrary.wiley.com/terms-and-conditions) on Wiley Online Library for rules of use; OA articles are governed by the applicable Creative Commons License

## 4. Discussion

### 4.1. Controls on the Timing of Peak Moulin Head

By constraining the timing of peak meltwater delivery to moulins within four GrIS catchments, we show that differences in the physical characteristics of catchments—area, snowpack extent, and supraglacial drainage efficiency—induce non-trivial heterogeneity in the timing of meltwater delivery to moulins. Lags between peak melting and peak meltwater delivery to moulins increased with catchment area (Figure 2a and Figure S14 in Supporting Information S1), resulting in longer delays in the timing of meltwater delivery to larger, higher-elevation catchments. This is expected because meltwater must be transported greater distances over the ice surface before reaching the catchment's terminal moulin (Sherman, 1932). Previous works have shown a positive relationship between catchment area and delays in meltwater delivery through applying terrestrial hydrological theory to supraglacial catchments throughout the GrIS ablation area (King, 2018; Smith et al., 2017; Yang & Smith, 2016; Yang et al., 2018). In considering 799 catchments in south west Greenland, Smith et al. (2017) showed that catchments with areas 0.4–245 $km^2$ could produce lags between peak melting and peak meltwater delivery to moulins of 0.4–9.5 hr. Our observations show that even a more limited range of catchment sizes (0.2–16.8 $km^2$) can induce differences of over 4 hr in the timing of meltwater delivery to moulins, thereby inducing a similar offset in timing of peak moulin head with increasing elevation in the ablation area.

The timing of meltwater delivery to moulins within individual catchments evolves over the course of the melt season as the seasonal snowpack melts and then as efficient supraglacial stream networks form (Lampkin & Vanderberg, 2014; Willis et al., 2002; Yang et al., 2018). The 2018 melt season began on 6 June when above-freezing air temperatures corresponded with an increase in surface ice velocity and tremor amplitude above winter-time background values (Figure S13 in Supporting Information S1). Early in the 2018 melt season (i.e., the first few weeks following the melt season's initiation on 6 June), snow cover was likely responsible for the longer residence time of meltwater within the supraglacial drainage system as indicated by the difference in peak tremor amplitude and peak sliding velocity between June and July (Figure 4). This longer residence time would have delayed meltwater delivery to the Low Camp moulin PIRA during the first few weeks of the 2018 melt season as the snowline quickly retreated upglacier (Text S9 in Supporting Information S1). This approximately 3 hr increase is similar to previous work on Haut Glacier d'Arolla's La Vierge catchment (0.11 $km^2$) where Willis et al. (2002) showed the seasonal snowpack could increase the lag between peak melting and peak meltwater delivery by more than 2 hr. Despite being snow-free by July 2018, peak meltwater delivery to PIRA moulin decreased by 1–1.75 hr between July and August. This shorter residence time of meltwater within the supraglacial drainage system is likely attributed to increased supraglacial drainage density where small tributaries drain into well-developed streams and rivers which quickly transport meltwater to the catchment's terminal moulin (e.g., Yang & Smith, 2016).

By including direct measurements of moulin head within the primary catchments considered in this study, we identified a 2 hr lag between peak meltwater delivery and peak moulin head. The lag between peak meltwater delivery and peak moulin head was consistent throughout the melt season and between sites despite significant differences in the magnitude and timing of peak meltwater delivery to the moulins themselves (Figures 2c and 2d). This contrasts previous assumptions that peak meltwater delivery to moulins and peak moulin head would occur simultaneously (e.g., McGrath et al., 2011). While our observations cannot be extrapolated to every moulin on the GrIS, they do demonstrate that there is a delay inherent to the coupled englacial-subglacial drainage system that controls the absolute timing of peak moulin head and therefore the timing of peak pressurization within moulin-connected parts of the subglacial drainage system.

### 4.2. Local Relationships Between Effective Pressure and Ice Motion

Lags between peak melting and peak sliding speed increased with elevation and distance from the ice sheet margin, echoing the pattern established by Hoffman et al. (2011). At Low Camp, peak moulin head and peak sliding speed were nearly coincident, indicating daily peaks in moulin head control the timing of peak subglacial water pressure and sliding. At High Camp, longer delays in meltwater delivery to our primary catchment's terminal moulin caused moulin head to peak 1–3.25 hr later than at Low Camp (Figure 3). However, this delay does not entirely account for the later timing of peak sliding, which lagged peak moulin head by up to 3.5 hr. Accordingly, the timing of peak moulin head was only partially responsible for the later timing of peak sliding.

19448007, 2022, 22, Downloaded from https://agupubs.onlinelibrary.wiley.com/doi/10.1029/2022GL100058, Wiley Online Library on [07/06/2023]. See the Terms and Conditions (https://onlinelibrary.wiley.com/terms-and-conditions) on Wiley Online Library for rules of use; OA articles are governed by the applicable Creative Commons License

Instead the timing offset between peak pressure within the moulin-connected drainage system and peak sliding speed indicates there is a difference in the relationship between effective pressure (ice overburden pressure minus subglacial water pressure) and sliding at higher elevations that was not observed lower on the ice sheet.

The spatial distribution and density of moulins control the development of the subglacial drainage system by determining where meltwater is delivered to the bed and thus where subglacial conduits form (Banwell et al., 2016; Gulley et al., 2012). When moulin head is high, subglacial conduits become pressurized relative to the surrounding distributed drainage system, driving water out laterally away from the conduits and into neighboring linked-cavities (Bartholomaus et al., 2007; Hubbard et al., 1995; Rada & Schoof, 2018; Werder et al., 2013). As higher pressures migrate out into the distributed system, basal traction is reduced over a larger area of the bed, thereby promoting sliding. Because sliding is controlled by the areally integrated basal traction over three to eight ice thicknesses (Gudmundsson, 2003), peak sliding should occur when high pressures cover the largest area of the bed. At lower elevations on the ice sheet where moulin density is high (e.g., Low Camp's primary catchment with more than 10 moulins per $km^2$; Figure S4 in Supporting Information S1), closely spaced subglacial conduits work in tandem to quickly pressurize a large area of the bed. However, at higher elevations where moulin density is much lower (e.g., High Camp with 1–3 moulins per $km^2$; Figure S5 in Supporting Information S1), sliding will be more coupled to the pressure change emanating from an individual conduit as it migrates into the distributed system. Modeling work by Werder et al. (2013) showed that the diurnal pressurization of a single conduit can extend up to 2 km into the distributed system, with the water pressure perturbation amplitude decreasing with distance away from the conduit, while also incurring a progressive phase lag of up to 6 hr. In this paradigm, the finite diffusion speed of the pressure change within the conduit at the base of High Camp's primary moulin could produce the 2 hr lag between peak moulin head and peak sliding observed at higher elevations on the ice sheet.

### 4.3. Implications

Our results reinforce previous observations of spatially inhomogeneous patterns of GrIS ice motion driven by areas with direct hydraulic connections to the bed, while highlighting the added complexity induced by the differences in timing of peak moulin head throughout the ablation area. Longitudinal flow coupling acts over a range of length-scales, explaining acceleration in areas of the GrIS without direct hydraulic connections to the bed (Price et al., 2008; Ryser et al., 2014). Areas without direct hydraulic connections (i.e., without moulins), respond passively to ice motion induced by pressure fluctuations within moulin-connected parts of the subglacial drainage system (Ryser et al., 2014). At our lower elevation site, moulin head and sliding speed peaked consistently earlier in the day than at higher elevations. Accordingly, when peak pressurization (or "slipperiness") was reached at these lower elevations, upglacier areas were still resisting flow, and vice versa. This observed offset in the timing of peak pressurization may then produce different patterns of ice deformation, stress transfer, and basal motion, than would be expected if the entire ablation area experienced peak pressurization coincidentally.

Alpine glaciers have been frequently used as analogs to the GrIS, yet their usefulness remains a point of debate. Fundamental relationships between hydrology and ice motion identified within alpine environments diverge with distance inland as the ice thickens, surface slopes flatten, and moulin density decreases. Our results demonstrate the correlation between peak moulin head and peak sliding initially identified on alpine glaciers (Iken, 1972) seems to hold at low to moderate elevations in areas with high moulin density (e.g., Low Camp). This relationship likely remains intact in this area because closely-spaced moulins are able to feed water to the entirety of the ice sheet bed simultaneously (Andrews et al., 2014). However, at higher elevations where moulin density is low (e.g., High Camp), the same correlation between peak moulin head and peak sliding is not observed. Accordingly, the straightforward coupling between effective pressure and ice motion derived from studies on alpine glaciers breaks down for inland reaches of the GrIS ablation area. Resolving the distinct processes governing hydrodynamic coupling within these areas will be more important as the GrIS ablation area continues to expand further inland as the climate warms (Noël et al., 2019).

## 5. Conclusions

Our observations suggest the supraglacial drainage system controls hydrodynamic coupling by two mechanisms: by creating delays in meltwater routing that propagate through the englacial and subglacial drainage systems and by controlling the spatial distribution of moulins which affects relationships between effective pressure

19448007, 2022, 22, Downloaded from https://agupubs.onlinelibrary.wiley.com/doi/10.1029/2022GL100058, Wiley Online Library on [07/06/2023]. See the Terms and Conditions (https://onlinelibrary.wiley.com/terms-and-conditions) on Wiley Online Library for rules of use; OA articles are governed by the applicable Creative Commons License

and sliding. Because moulin density and catchment area are inherently linked, these processes work together to produce the progressively later timing daily peak sliding speeds with increasing distance from the ice sheet's margin. Given the role of the supraglacial drainage system in controlling the timing of peak subglacial pressurization, we would expect the well-documented heterogeneity of supraglacial catchments (King, 2018; Smith et al., 2017; Yang & Smith, 2016) to produce widespread variability in the timing of peak pressurization experienced within different regions of the subglacial drainage system. How these complex patterns of subglacial pressurization influence ice flow need to be considered in order to determine how the GrIS will respond to increased melting under future climatic warming.

## Data Availability Statement

The data sets and code used in this study are openly available. Meteorological and hydrological data sets are archived with the National Science Foundation's Arctic Data Center through the MoVE project's portal: http://arcticdata.io/catalog/portals/moulin (Mejia, Trunz, Covington, & Gulley, 2020; Mejia, Trunz, Covington, Gulley, & Breithaupt, 2020). Greenland Climate Network weather station data from JAR1 is available from (Steffen et al., 1996) and is also archived with (Mejia, Trunz, Covington, & Gulley, 2020) for convenience. Data from our on-ice GNSS stations and the base stations used during processing are archived through UNAVCO's GAGE Facility (Fahnestock et al., 2006; Mejia, Gulley, & Dixon, 2020). The Python module created to pick diurnal extrema from timeseries data is archived with Zenodo (see Mejia, 2022).

**Acknowledgments**

This work was supported by the United States National Science Foundation Grant 1604022. GNSS station support was provided by UNAVCO in collaboration with the National Science Foundation. We acknowledge and would like to thank Victoria Siegel and Ronald Knoll for assistance in the field. Polar Field Services, Inc. provided logistical support, and special thanks to Kathy Young for her work supporting field campaigns. ArcticDEM provided by the Polar Geospatial Center under NSF-OPP awards 1043681, 1559691, and 1542736. DEM(s) were created from DigitalGlobe, Inc., imagery and funded under National Science Foundation awards 1043681, 1559691, and 1542736. We would also like to thank the two reviewers whose comments and suggestions greatly improved the quality of the manuscript.

## References

Andrews, L. C., Catania, G. A., Hoffman, M. J., Gulley, J. D., Lüthi, M. P., Ryser, C., et al. (2014). Direct observations of evolving subglacial drainage beneath the Greenland Ice Sheet. *Nature*, *514*(7520), 80–83. https://doi.org/10.1038/nature13796

Andrews, L. C., Hoffman, M. J., Neumann, T. A., Catania, G. A., Luthi, M. P., Hawley, R. L., et al. (2018). Seasonal evolution of the subglacial hydrologic system modified by supraglacial lake drainage in Western Greenland. *Journal of Geophysical Research: Earth Surface*, *123*(6), 1479–1496. https://doi.org/10.1029/2017JF004585

Badino, G., & Piccini, L. (2002). Englacial water fluctuation in moulins: An example from Tyndall glacier (Patagonia, Chile). *Nimbus*, *23–24*, 125–129.

Banwell, A. F., Hewitt, I. J., Willis, I. C., & Arnold, N. S. (2016). Moulin density controls drainage development beneath the Greenland Ice Sheet. *Journal of Geophysical Research: Earth Surface*, *121*(12), 2248–2269. https://doi.org/10.1002/2015JF003801

Bartholomaus, T. C., Anderson, R. S., & Anderson, S. P. (2007). Response of glacier basal motion to transient water storage. *Nature Geoscience*, *1*, 33–37. https://doi.org/10.1038/ngeo.2007.52

Bartholomaus, T. C., Larsen, C. F., Amundson, J. M., O'Neel, S., Walter, J. I., & West, M. E. (2015). Subglacial discharge at tidewater glaciers revealed by seismic tremor. *Geophysical Research Letters*, *42*(15), 6391–6398. https://doi.org/10.1002/2015GL064590

Clason, C. C., Mair, D. W., Nienow, P. W., Bartholomew, I., Sole, A. J., Palmer, S., & Schwanghart, W. (2015). Modelling the transfer of supraglacial meltwater to the bed of Leverett glacier, Southwest Greenland. *The Cryosphere*, *9*(1), 123–138. https://doi.org/10.5194/tc-9-123-2015

Covington, M. D., Gulley, J. D., Trunz, C., Mejia, J., & Gadd, W. (2020). Moulin volumes regulate subglacial water pressure on the Greenland Ice Sheet. *Geophysical Research Letters*, *47*(20), e2020GL088901. https://doi.org/10.1029/2020GL088901

de Fleurian, B., Morlighem, M., Seroussi, H., Rignot, E., van den Broeke, M. R., Kuipers Munneke, P., et al. (2016). A modeling study of the effect of runoff variability on the effective pressure beneath Russell glacier, West Greenland. *Journal of Geophysical Research: Earth Surface*, *121*(10), 1834–1848. https://doi.org/10.1002/2016JF003842

Fahnestock, M. A., Truffer, M., Sdfe, T. D. A., & Community, U. (2006). Greenland GNSS network—KAGA-Kangia North P.S. UNAVCO. https://doi.org/10.7283/FQGY-4535

Gimbert, F., Tsai, V. C., Bartholomaus, T. C., Amundson, J. M., & Walter, J. I. (2016). Subseasonal changes observed in subglacial channel pressure, size, and sediment transport. *Geophysical Research Letters*, *43*(September), 3786–3794. https://doi.org/10.1002/2016GL068337

Gudmundsson, G. H. (2003). Transmission of basal variability to a glacier surface. *Journal of Geophysical Research*, *108*(B5), 1–19. https://doi.org/10.1029/2002jb002107

Gulley, J. D., Grabiec, M., Martin, J. B., Jania, J., Catania, G. A., & Glowacki, P. S. (2012). The effect of discrete recharge by moulins and heterogeneity in flow-path efficiency at glacier beds on subglacial hydrology. *Journal of Glaciology*, *58*(211), 926–940. https://doi.org/10.3189/2012JoG11J189

Hoffman, M. J., Catania, G. A., Neumann, T. A., Andrews, L. C., & Rumrill, J. A. (2011). Links between acceleration, melting, and supraglacial lake drainage of the Western Greenland Ice Sheet. *Journal of Geophysical Research*, *116*(4), 1–16. https://doi.org/10.1029/2010JF001934

Hubbard, B., Sharp, M. J., Willis, I. C., Nielsen, M. K., & Smart, C. (1995). Borehole water-level variation and the structure of the subglacial hydrological system of haut glacier d'Arolla, Valais, Switzerland. *Journal of Glaciology*, *41*(139), 572–583. https://doi.org/10.1017/s0022143000034894

Iken, A. (1972). Measurements of water pressure in moulins as part of A movement study of the white glacier, Axel Heiberg Island, Northwest territories, Canada. *Journal of Glaciology*, *11*(61), 53–58. https://doi.org/10.3189/s0022143000022486

King, L. A. (2018). *Identifying and characterizing the spatial variability of supraglacial hydrological features on the western Greenland Ice Sheet Doctoral dissertation*. University of British Columbia. https://doi.org/10.14288/1.0372827

Lampkin, D. J., & Vanderberg, J. (2014). Supraglacial melt channel networks in the Jakobshavn Isbræ region during the 2007 melt season. *Hydrological Processes*, *28*(25), 6038–6053. https://doi.org/10.1002/hyp.10085

McGrath, D., Colgan, W. T., Steffen, C., Lauffenburger, P., & Balog, J. (2011). Assessing the summer water budget of a moulin basin in the sermeq avannarleq ablation region, Greenland Ice Sheet. *Journal of Glaciology*, *57*(205), 954–964. https://doi.org/10.3189/002214311798043735

Mejia, J. Z. (2022). DiurnalExtrema. Zenodo, v1.0.0. https://doi.org/10.5281/zenodo.6812156

Mejia, J. Z., Gulley, J. D., & Dixon, T. H. (2020). *West Greenland moulins 2017–2019 Sermeq Avannarleq—GPS/GNSS observations data set*. The GAGE Facility operated by UNAVCO, Inc. https://doi.org/10.7283/VT31-EK40

Mejia, J. Z., Gulley, J. D., Trunz, C., Covington, M. D., Bartholomaus, T. C., Xie, S., & Dixon, T. (2021). Isolated cavities dominate Greenland Ice Sheet dynamic response to lake drainage. *Geophysical Research Letters*, *48*(19), 1–11. https://doi.org/10.1029/2021gl094762

Mejia, J. Z., Trunz, C., Covington, M. D., & Gulley, J. D. (2020). *Meteorological data from two on-ice weather stations at 780 and 950 m asl elevations in the ablation area of Sermeq Avannarleq, West Greenland from 2017-2018*. Arctic Data Center. https://doi.org/10.18739/A2CF9J745

Mejia, J. Z., Trunz, C., Covington, M. D., Gulley, J. D., & Breithaupt, C. (2020). *Moulin hydrological measurements from Sermeq Avannarleq, West Greenland ice sheet from 2017-2018*. Arctic Data Center. https://doi.org/10.18739/A2M03XZ13

Morlighem, M., Williams, C. N., Rignot, E., An, L., Arndt, J. E., Bamber, J. L., et al. (2017). BedMachine v3: Complete bed topography and ocean bathymetry mapping of Greenland from multibeam echo sounding combined with mass conservation. *Geophysical Research Letters*, *44*(21), 11051–11061. https://doi.org/10.1002/2017GL074954

Noël, B., van de Berg, W. J., Lhermitte, S., & van den Broeke, M. R. (2019). Rapid ablation zone expansion amplifies north Greenland mass loss. *Science Advances*, *5*(9), 2–11. https://doi.org/10.1126/sciadv.aaw0123

Pellicciotti, F., Brock, B., Strasser, U., Burlando, P., Funk, M., & Corripio, J. (2005). An enhanced temperature - Index glacier melt model including the shortwave radiation balance: Development and testing for Haut Glacier d'Arolla, Switzerland. *Journal of Glaciology*, *51*(175), 573–587. https://doi.org/10.3189/172756505781829124

Price, S. F., Payne, A. J., Catania, G. A., & Neumann, T. A. (2008). Seasonal acceleration of inland ice via longitudinal coupling to marginal ice. *Journal of Glaciology*, *54*(185), 213–219. https://doi.org/10.3189/002214308784886117

Rada, C., & Schoof, C. (2018). Channelized, distributed, and disconnected: Subglacial drainage under a valley glacier in the Yukon. *The Cryosphere*, *12*(8), 2609–2636. https://doi.org/10.5194/tc-12-2609-2018

Rennermalm, Å. K., Moustafa, S. E., Mioduszewski, J., Chu, V. W., Forster, R. R., Hagedorn, B., et al. (2013). Understanding Greenland ice sheet hydrology using an integrated multi-scale approach. *Environmental Research Letters*, *8*(1), 015017. https://doi.org/10.1088/1748-9326/8/1/015017

Ryser, C., Lüthi, M. P., Andrews, L. C., Catania, G. A., Funk, M., Hawley, R. L., et al. (2014). Caterpillar-like ice motion in the ablation zone of the Greenland ice sheet. *Journal of Geophysical Research: Earth Surface*, *119*(10), 2258–2271. https://doi.org/10.1002/2013JF003067

Sherman, L. K. (1932). The relation of hydrographs of runoff to size and character of drainage-basins. *Eos, Transactions American Geophysical Union*, *13*(1), 332–229. https://doi.org/10.1029/tr013i001p00332

Smith, L. C., Chu, V. W., Yang, K., Gleason, C. J., Pitcher, L. H., Rennermalm, Å. K., et al. (2015). Efficient meltwater drainage through supraglacial streams and rivers on the southwest Greenland ice sheet. *Proceedings of the National Academy of Sciences*, *112*(4), 1001–1006. https://doi.org/10.1073/pnas.1413024112

Smith, L. C., Yang, K., Pitcher, L. H., Overstreet, B. T., Chu, V. W., Rennermalm, Å. K., et al. (2017). Direct measurements of meltwater runoff on the Greenland ice sheet surface. *Proceedings of the National Academy of Sciences*, *114*(50), 1–10. https://doi.org/10.1073/pnas.1707743114

Steffen, C., Box, J. E., & Abdalati, W. (1996). Greenland climate network: GC-net. Cold regions Research and engineering laboratory, CRREL spec, 98–103. Retrieved from https://books.google.com/books?hl=en%26lr=%26id=m4zuBvzFn60C%26oi=fnd%26pg=PA98%26dq=steffen+gc-net%26ots=qqL-M_8kva%26sig=Cacykn6f3zXUnAYnDpaIG55Wbpw#v=onepage%26q=steffen%20gc-net%26f=false

Trunz, C., Mejia, J., Covington, M., Siegel, V., Conlon, B., & Gulley, J. D. (2021). Supraglacial stream discharge measurements from six catchments within the Pâqitsoq region of Sermeq Avannarleq, Western Greenland Ice Sheet 2017–2018. *Arctic Data Center*. https://doi.org/10.18739/A2D21RK53

Werder, M. A., Hewitt, I. J., Schoof, C., & Flowers, G. E. (2013). Modeling channelized and distributed subglacial drainage in two dimensions. *Journal of Geophysical Research: Earth Surface*, *118*(4), 2140–2158. https://doi.org/10.1002/jgrf.20146

Willis, I. C., Arnold, N. S., & Brock, B. W. (2002). Effect of snowpack removal on energy balance, melt and runoff in a small supraglacial catchment. *Hydrological Processes*, *16*(14), 2721–2749. https://doi.org/10.1002/hyp.1067

Yang, K., & Smith, L. C. (2016). Internally drained catchments dominate supraglacial hydrology of the southwest Greenland Ice Sheet. *Journal of Geophysical Research: Earth Surface*, *121*(10), 1891–1910. https://doi.org/10.1002/2016JF003927

Yang, K., Smith, L. C., Karlstrom, L., Cooper, M. G., Tedesco, M., van As, D., et al. (2018). A new surface meltwater routing model for use on the Greenland Ice Sheet surface. *The Cryosphere*, *12*, 3791–3811. https://doi.org/10.5194/tc-12-3791-2018

## References From the Supporting Information

Conrad, O., Bechtel, B., Bock, M., Dietrich, H., Fischer, E., Gerlitz, L., et al. (2015). System for automated geoscientific Analyses (SAGA) v. 2.1.4. *Geoscientific Model Development*, *8*(7), 1991–2007. https://doi.org/10.5194/gmd-8-1991-2015

Herring, T., King, R. W., & McClusky, S. C. (2010). Introduction to GAMIT/GLOBK. Massachusetts Institute of Technology.

Kilpatrick, F. A., & Cobb, E. D. (1985). Measurement of discharge using tracers. In *Techniques of water-resources investigations of the United States geological survey*. (Vol. 3, pp. 1–52). Book.

Porter, C., Morin, P., Howat, I., Noh, M.-J., Bates, B., Peterman, K., et al. (2018). ArcticDEM. *Harvard Dataverse*. https://doi.org/10.7910/DVN/OHHUKH

Röösli, C., Walter, F., Husen, S., Andrews, L. C., Luthi, M. P., Catania, G. A., & Kissling, E. (2014). Sustained seismic tremors and icequakes detected in the ablation zone of the Greenland ice sheet. *Journal of Glaciology*, *60*(221), 563–575. https://doi.org/10.3189/2014JoG13J210

Wang, L., & Liu, H. (2006). An efficient method for identifying and filling surface depressions in digital elevation models for hydrologic analysis and modelling. *International Journal of Geographical Information Science*, *20*(2), 193–213. https://doi.org/10.1080/13658810500433453

Xie, S., Law, J., Russell, R., Dixon, T. H., Lembke, C., Malservisi, R., et al. (2019). Seafloor geodesy in shallow water with GPS on an Anchored Spar Buoy. *Journal of Geophysical Research: Solid Earth*, *124*(11), 12116–12140. https://doi.org/10.1029/2019JB018242



19448007, 2022, 22, Downloaded from https://agupubs.onlinelibrary.wiley.com/doi/10.1029/2022GL100058, Wiley Online Library on [07/06/2023]. See the Terms and Conditions (https://onlinelibrary.wiley.com/terms-and-conditions) on Wiley Online Library for rules of use; OA articles are governed by the applicable Creative Commons License